Remote Sensing of Environment 216 (2018) 647–657

Contents lists available at ScienceDirect

Remote Sensing of Environment

journal homepage: www.elsevier.com/locate/rse

Estimating smallholder crops production at village level from Sentinel-2 time series in Mali's cotton belt

Marie-Julie Lambert[a,*], Pierre C. Sibiry Traoré[b,c], Xavier Blaes[a], Philippe Baret[a], Pierre Defourny[a]

[a] Earth and Life Institute, Université catholique de Louvain, Croix du Sud 2, 1348 Louvain-la-Neuve, Belgium
[b] MANOBI S.A., Fenêtre Mermoz V. 17, Dakar-Fann BP 25026, Senegal
[c] International Crops Research Institute for the Semi-Arid Tropics (ICRISAT), Samanko Stn., Bamako POB 320, Mali

ARTICLE INFO

Keywords:
Sentinel-2
Crop production
Smallholder agriculture
Cotton belt
Mali

ABSTRACT

In Mali's cotton belt, spatial variability in management practices, soil fertility and rainfall strongly impact crop productivity and the livelihoods of smallholder farmers. To identify crop growth conditions and hence improve food security, accurate assessment of local crop production is key. However, production estimates in heterogeneous smallholder farming systems often rely on labor-intensive surveys that are not easily scalable, nor exhaustive. Recent advances in high-resolution earth observation (EO) open up new possibilities to work in heterogeneous smallholder systems. This paper develops a method to estimate individual crop production at farm-to-community scales using high-resolution Sentinel-2 time series and ground data in the commune of Koningue, Mali. Our estimation of agricultural production relies on (i) a supervised, pixel-based crop type classification inside an existing cropland mask, (ii) a comparison of yield estimators based on spectral indices and derived leaf area index (LAI), and (iii) a Monte Carlo approach combining the resulting unbiased crop area estimate and the uncertainty on the associated yield estimate. Results show that crop types can be mapped from Sentinel-2 data with 80% overall accuracy (OA), with best performances observed for cotton (Fscore 94%), maize (88%) and millet (83%), while peanut (71%) and sorghum (46%) achieve less. Incorporation of parcel limits extracted from very high-resolution imagery is shown to increase OA to 85%. Obtained through inverse radiative transfer modeling, Sen2-Agri estimates of LAI achieve better prediction of final grain yield than various vegetation indices, reaching R^2 of 0.68, 0.62, 0.8 and 0.48 for cotton, maize, millet and sorghum respectively. The uncertainty of Monte Carlo production estimates does not exceed 0.3% of the total production for each crop type.

1. Introduction

In Mali's cotton belt, smallholder farming systems face soil fertility challenges, demographic, and environmental pressures that affect farmers' livelihoods and food security (Karlson and Ostwald, 2015; Potts et al., 2013). Crop production fluctuates strongly in time and space and leads to chronic food insecurity (Akponikpe et al., 2011). Smallholder rainfed agricultural systems host more than 50% of the rural population in developing countries and yet produce 90% of the food (Morton, 2007). While smallholder farming systems differ widely between countries and agro-ecological zones, they often share common features such as limited resource endowment, labor scarcity, low productivity of labor, high productivity of capital and risk management in economic decisions (Dixon et al., 2004; Cousins, 2010). In developing countries, food security assessments often rely on early warning systems (EWS) based on Normalized Difference Vegetation Index (NDVI) anomalies. Such systems offer food security alerts at medium spatial resolution that are not detailed enough to detect the emergence of local food insecurity conditions, and often leverage remote sensing only in a qualitative sense (Baruth et al., 2008). Meanwhile, the generation of agricultural statistics (area, yield and production) relies almost exclusively on labor-intensive field surveys that are both constrained regarding representativeness and reliability. Recent instances of EWS failing to identify the emergence of localized famines in Ethiopia (1999–2000), Malawi (2001–2002) and Niger (2005) (Genesio et al., 2011; Devereux, 2009), highlight the outstanding challenges faced by EWS in assessing local food insecurity, including data accuracy, timeliness and disaggregation. For example, the 1999–2000 Ethiopian famine was concentrated in the lowland pastoralist areas, while EWS mainly focused on the crop-producing highlands (Maxwell, 2002).

Recent improvements in the spatial, spectral and temporal resolutions of EO satellites hold significant potential for improved food

* Corresponding author.
E-mail address: lambertmariejulie@gmail.com (M.-J. Lambert).

https://doi.org/10.1016/j.rse.2018.06.036
Received 30 September 2017; Received in revised form 15 June 2018; Accepted 24 June 2018

security assessments. Remote sensing applications traditionally face considerable challenges in smallholder agriculture because of small field size, heterogeneity in management practices, the resulting landscape fragmentation, and the widespread presence of trees within the fields (Delrue et al., 2013; Vancutsem et al., 2012). Some studies achieved accurate land cover classifications of smallholder farming systems using high-resolution (HR) imagery (Sweeney et al., 2015), very high-resolution (VHR) imagery (Debats et al., 2016) or a combination thereof (Lebourgeois et al., 2017). While some authors deemed VHR compulsory for such purposes (Lebourgeois et al., 2017; McCarty et al., 2017), others found HR to be sufficient (Pervez et al., 2014). Settling this question is probably context-specific. Results from Leroux et al. (2014) in a similar and nearby agro-ecology suggest that a 10-m spatial resolution may suffice for land cover classification in the Malian cotton belt.

Quantitative estimates of smallholder yields from EO also offer potential to improve scalability and objectivity, compared to estimates generated from survey data. Two popular approaches used to estimate crop yield from EO include (i) empirical models based on regressions between yield measurements and spectral VIs and, (ii) crop growth models involving the use of weather, soil, plant, management and satellite data. In theory, the agility of crop models featuring a finer-scale representation of plant, soil and management processes confers them a higher accuracy for yield estimation. In practice, however, they are constrained by data availability (Morel et al., 2014; Burke and Lobell, 2017) and lack of granularity, and are biased towards temperate, high-yielding cultivars (Srivastava et al., 2016; Gaiser et al., 2010). EO-derived yield predictors, on the other hand, evaluate actual precursors of yield and can be applied at granular scales increasingly congruent with the reality of smallholder agricultural systems. A set of recent studies (Schut et al., 2018; Jin et al., 2017; Han et al., 2017; Azzari et al., 2017; Burke and Lobell, 2017; Jain et al., 2016) focused on yield estimation from EO. Chivasa et al. (2017) suggested that the decreasing cost of EO data opens opportunities for maize yield estimation in heterogeneous African agricultural landscapes, but that reliable field data and accurate classification methods remain key. Jin et al. (2017) compared an empirically calibrated model using yield measurements and an uncalibrated model based on pseudo training data generated from a crop model. At an aggregated administrative scale (*e.g.*, district and division), the calibrated and uncalibrated models reach similar performances with R^2 ranging from 0.3 to 0.6 in both cases. Achieving robust smallholder landscape yield predictions is important in sub-Saharan Africa, notably where subsistence agriculture still determines food security, and for profitable farmer participation in more contract-oriented agricultural areas. These yield predictions should also be robust at an individual crop level, to adequately represent the diversity of food and income sources, and for economic efficiency should attempt to leverage as much value as possible from open-source, free data.

This research aims to propose an integrated method to estimate crops production at local community scale, and uncertainty thereof, in complex and heterogeneous smallholder farming systems. It involves the field-level mapping of crop type using supervised pixel-based classification, the identification of a best crop-specific yield estimator from a temporally reduced set of vegetation status proxies (vegetation indices and LAI), and a stochastic combination of these two results and their respective uncertainties. The approach, based on Sentinel-2 EO data, is tested in 2016 in a rural commune of the Koutiala district in Mali's cotton belt.

2. Study site

The study area (353 km^2) is defined by the geographical footprint of the 43 farmers associations registered in the five villages of the Koningue commune (Koutiala district, South-Eastern Mali): Dougan, Sukumba, Ngueguesso 1, Ngueguesso 2 and Banesso (Fig. 1). The site is located in the older cotton production basin of Mali, characterized by relatively high population density (by Malian standards), land saturation, fragmentation, and degradation. The area also features a relatively strong legacy of agricultural extension, spearheaded since 1974 by the cotton parastatal, Compagnie Malienne de Développement des Textiles (CMDT). Extension services provide access to subsidized inputs, an outlet for the sale of cotton production, and agronomic advice that covers the entire cropping system including other main crops like maize, millet, peanut, and sorghum. The combination of these factors results in a relatively advanced state of agricultural intensification, albeit with large heterogeneity in production levels from landscape to community scales.

Average annual rainfall reaches 890-mm with high inter-annual and intra-seasonal variability. Precipitations are very dominantly convective, inducing high spatial heterogeneity at the local scale (Breusers, 2004) especially towards the tails of the season. Soil properties follow the catena, with high plateaus presenting moderately deep, argillic soils, midslopes featuring moderately deep to shallow, gravelly and lateritic soils (Cuirustalfs, Mollic Cuirorthents, Lithic Haplustalfs), and deep, well drained and moderately fine textured soils in the lowlands (Plintic/Ultic Haplustalfs, Oxic Haplustults) (Diallo and Keita, 1995; Blaes et al., 2016). Local farmers distinguish five soil types (Fig. 1): ‘*fara dugu kolo*’, rocky soils located on plateaus and slopes; (2) ‘*bele dugu kolo*’, red gravelly soils located on plateaus; (3) ‘*cencen dugu kolo*’, sandy soils located on slopes and lowlands; (4) ‘*bogo dugu kolo*’, loamy soils located in lowlands; and, (5) ‘*mana dugu kolo*’, lowlands clayey soils.

Cotton (*Gossypium* sp.), maize (*Zea mays* L. ssp.), sorghum (*Sorghum bicolor* (L.) Moench) and pearl millet (*Pennisetum glaucum* (L.) R. Br.) are the main crops in the region. The growing season starts with the first rains around May and crops are harvested from early September (maize) to end of November (millet) (Fig. 2). CMDT organizes cotton production with farmer organizations, which strongly impacts local livelihoods as cotton is the main cash crop (Baffes, 2007). Sorghum, millet and peanut are cultivated mainly for household consumption. Since a few years, different studies highlighted the ‘*maizification*’ of the area (Laris et al., 2015; Falconnier, 2009). The maize crop has several advantages over other local grains: higher yields, easier to sell, and rapid maturation allowing early harvest during the lean season. However, it requires more fertilizer and is more susceptible to drought than sorghum and millet.

3. Data

3.1. Satellite imagery

Sentinel-2A time series for the 2016 season (temporal resolution of 10 days) was processed to level L2A following Sentinel-2 for Agriculture (Sen2-Agri) protocols (Bontemps et al., 2015) (http://www.esa-sen2agri.org/). The MACCS algorithm uses the multi-temporal dimension of the Sentinel-2 time series to detect clouds and shadows, correct atmospheric perturbations and retrieve aerosol optical thickness (Hagolle et al., 2015,2010). From the 12 Sentinel-2A images acquired during the 2016 growing season, six were discarded due to cloud cover exceeding 50%. The remaining six images (27-07, 26-08, 05-09, 05-10, 25-10, 14-11) were used for crop type mapping and yield estimation. Within these images, local outstanding gaps due to cloud and shadow filtering were filled in by linear temporal interpolation. Additionally, a cloud-free WorldView-3 image at 1.24-m multispectral resolution was acquired on 9 October 2016.

3.2. Secondary data

Secondary thematic data layers were provided by ICRISAT, a partner in the 2014–2017 STARS project (Spurring a Transformation for Agriculture through Remote Sensing) active in our study area. These included 2014 and 2015 seasonal time series of VHR DigitalGlobe

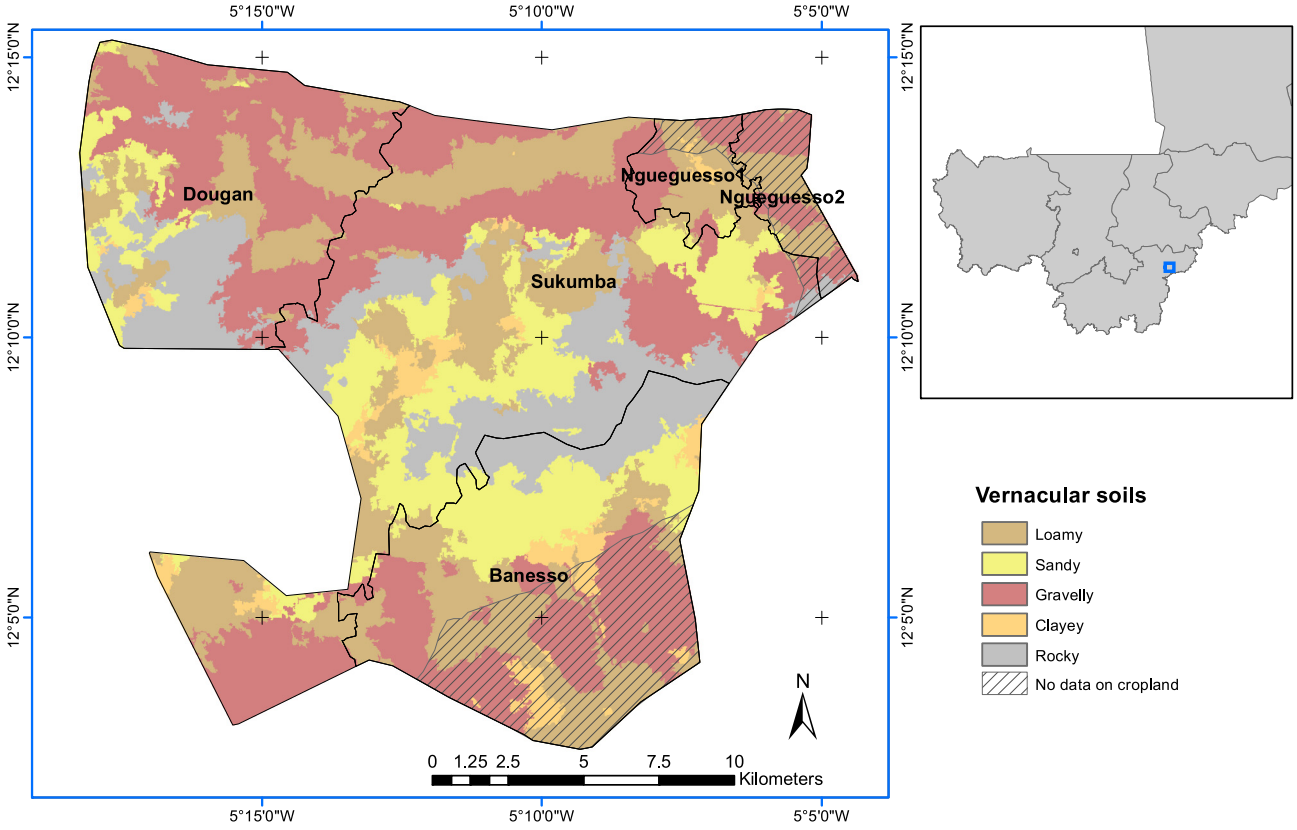

Fig. 1. The Koningue commune with the five village areas. The vernacular soil map is shown as background and produced combining geolocalized vernacular soils information and EO data providing soil brightness and elevation. Parcel boundaries are available on the entire study area except for the southern part of the Banesso and Ngueguesso 2 communities (stripped black lines). Source: Traroé et al (2015).

imagery, used in STARS to, *inter alia*, (i) exhaustively delineate 31,248 agricultural parcels and generate annual cropland masks; (ii) derive a landscape-level tree mask from soil-specific NDVI thresholding of a 2014 early-season WorldView-2 image (Blaes et al., 2016); and (iii) a concomitant digital dataset on vernacular soil types collected from farmer interviews (6700 + georeferenced samples).

We used these secondary datasets to, respectively (i) update parcels database and resulting cropland maps for 2016, by photointerpretation of the additional DigitalGlobe coverage acquired on 9 October 2016, and setting the 2016 cropland extent to a total 156 km^2 over the study area; and (ii) generate a vernacular soil map from the combination of STARS farmer interview data, object-based segmentation of a Sentinel-2 derived soil brightness image, and Shuttle Radar Topography Mission (SRTM) 30-m elevation digital elevation model.

3.3. In situ data

A set of 821 crop type georeferenced points were collected on the ground in October and November 2016, and included six classes: cotton, maize, millet, sorghum, peanut, and other (*e.g.* soybean). Encompassing field boundaries were digitized on the VHR WorldView-3 image of 9/10/2016 for each of the geo-referenced points. Among the 821 resulting polygons, cotton came out as the dominant crop. It is followed by millet, maize and sorghum covering 23.7%, 20.2% and 10.1% respectively. Peanut and other crops are minor contributors, occupying less than 3% of the sampled area.

We measured total aboveground biomass (AGB) and grain yield on a subset of 105 fields for the four dominant crop types (26 cotton, 27 millet, 27 sorghum and 25 maize), with 3 measurement replications per field. Field selection followed a stratified sampling approach based on catena position (plateau, slope and valley) and household endowment level (low, medium, high), derived from local expert knowledge. There were three fields per crop species in each of the nine strata. The slightly smaller sample of maize and cotton fields was due to unexpected early harvest by a couple of farmers. On each field, the operator physically verified the field perimeter with the farmer, recording the boundaries

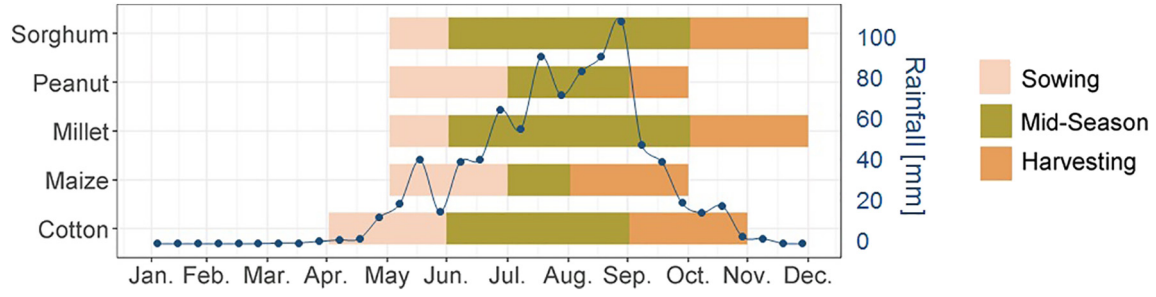

Fig. 2. Crop calendar of dominant crops in the cotton belt region with decadal rainfall for the 2016 year. Rainfall data source: http://dataviz.vam.wfp.org/.

Table 1
Vegetation indices (VI) selected for crop yield estimation.

VI	Formulation	Ref
Green VI		
NDVI	$NDVI = \frac{\rho Nir - \rho Red}{\rho Nir + \rho Red}$	Rouse Jr. et al. (1974)
Green NDVI	$gNDVI = \frac{\rho Nir - \rho Green}{\rho Nir + \rho Green}$	Gitelson et al. (1996)
Red-edge NDVI	$NDVIre = \frac{\rho Nir - \rho Red-Edge}{\rho Nir + \rho Red-Edge}$	Gitelson and Merzlyak (1994)
Chlorophyles indices		
Green Chlorophyll Index	$Cl_{Green} = \frac{\rho Nir}{\rho Green} - 1$	Gitelson et al. (2003)
Red-edge Chlorophyll Index	$Cl_{Red-edge} = \frac{\rho Red-edge}{\rho Green} - 1$	Gitelson et al. (2003)
Modified Chlorophyll Absorption Ratio Index	$MCARI2 = \frac{1.5[2.5*(\rho Nir - \rho red) - 1.3(\rho Nir - \rho Green)]}{\sqrt{(2\rho Nir + 1)^2 - (6\rho Nir - 5\sqrt{\rho red}) - 0.5}}$	Haboudane et al. (2004)
Triangular Vegetation Index	$TVI = 0.5[120(\rho_{Red} - \rho_{Green}) - 200(\rho_{red} - \rho_{Green})]$	Broge and Leblanc (2001)
Modified Triangular Vegetation Index	$MTVI2 = \frac{1.5[1.2*(\rho Nir - \rho Green) - 2.5(\rho red - \rho Green)]}{\sqrt{(2\rho Nir + 1)^2 - (6\rho Nir - 5\sqrt{\rho red}) - 0.5}}$	Haboudane et al. (2004)
Dry biomass indices		
Soil Tillage Index	$STI = \frac{\rho Swir1}{\rho Swir2}$	Van Deventer et al. (1997)
Normalized Difference Tillage Index	$NDTI = \frac{\rho Swir1 - \rho Swir2}{\rho Swir1 + \rho Swir2}$	Van Deventer et al. (1997)
LAI	Sen2-Agri System	Weiss and Baret (1999)

with a Trimble Juno 5 GPS. Within each field, three quadrats of 4-m^2 were randomly selected for destructive sampling, subject to a separation distance of 20-m from the nearest tree crown or field boundary (to avoid edge effects). Grain yield was estimated based on a threshing ratio (weight of grain over weight of ear/panicle) of 0.6, 0.75 and 0.85 for maize, millet and sorghum respectively (Ajeigbe, 2017 and Gangashetty, 2017, *pers. comm.*). Cottonseed weight was determined directly, so no conversion ratio was applied.

4. Methodology

The overall approach involves three main steps: (i) mapping crop type within the existing cropland mask, and estimating unbiased crop area; (ii) predicting the yield of individual crops; and (iii) estimating aggregate production, crop-wise with associated uncertainties accounting for both crop map and yield model errors.

4.1. Crop type classification and crop area estimation

We used a pixel-based, supervised Random Forest (RF) classification to discriminate main crop types within the cropland area. The reference 821 ground dataset (totaling 131,424 pixels) was split into spatially uncorrelated training (2/3) and validation (1/3) subsets following a stratified random sampling (strata being crop types). For the training sample, a 10-m internal buffer was applied on VHR-extracted field boundaries to reduce the number of mixels (that constraint was not applied on the validation sample to avoid accuracy overestimation).

The RF classifier used all Sentinel-2 bands resampled to 10-m except the blue, which was discarded due to the impact of aerosols and atmospheric scattering (Jia et al., 2014). The RF classifier was chosen based on its lack of over-fitting, its parsimony for user-defined parameters, the features importance analysis, its low sensitivity to the number of inputs, its minimization of correlations between classifiers, its light computational requirements, and its robustness to noise and overtraining (Rodriguez-Galiano et al., 2012; Hastie et al., 2009; Gislason et al., 2006). The number of trees was set to 500 following Rodriguez-Galiano et al. (2012).

To assess the most relevant combination of band and date (a.k.a '*feature*') for crop type discrimination, we computed the mean decrease in Gini Index for each feature. To calculate feature importance, the RF algorithm turns off one of the feature while maintaining the others constant and assesses the decrease in accuracy with the Gini Index. The feature has the highest importance when the mean decrease in Gini Index is the largest (Breiman, 2001).

A majority voting was applied on the resulting pixel classification using the VHR-derived cropland vector layer and the SpatialEco R package (https://www.rdocumentation.org/packages/spatialEco), and we computed overall accuracy (OA) at both pixel and parcel levels; user accuracy (UA), producer accuracy (PA) and Fscore for each crop type were computed at parcel level only $\left(Fscore = \frac{2*PA*UA}{PA+UA}\right)$.

To generate an unbiased area estimate per crop, we used a direct calibration estimator of the area, relying on ground truth to remove the bias of the classified map following Gallego (2004). In the confusion matrix, the conditional probability $P(j|i)$ is the probability to be j (ground truth) when classified as i, with j and $i \in$ (*cotton,maize,-millet,sorghum*). The unbiased area is determined by the Eq. (1).

$$A_j = \sum_{i=1}^{4} (A_i * P(j|i)) \quad (1)$$

Where A_j is the unbiased area of crop j, A_i is the area of pixels classified as i assuming that each pixel covers an area of 100 m^2, and $P(j|i)$ is the conditional probability to be j when knowing i.

Additionally, as farmers actively preserve numerous trees inside crop fields for their commercial and soil fertility maintenance values (Traoré et al., 2002; Traoré, 2003) including notably shea (*Vitellaria paradoxa*) and néré (*Parkia biglobosa*), we investigated the effect of tree exclusion on crop classification accuracies, considering the low rates of changes of tree cover associated with active farmer preservation and slow growth rates. The 2014 pre-existing STARS 2-m tree mask was resampled to 10-m resolution, with resulting pixels considered as being trees if tree coverage therein exceeded 20% (to limit the effects of tree shadows and imperfect co-registration between images). Photo-interpretation of the WorldView-3 image of 9 October 2016 validated this coarser tree mask against 150 randomly selected pixels classified as tree (100) or non-tree (50). The overall accuracies and their respective standard deviations were computed to compare the performance of crop type classifications with and without trees (Rossiter, 2004). Finally, the resulting crop type map was used to explore the relationship between soil type and crop type.

4.2. Yield estimation

Table 1 references the various spectral vegetation indices (VIs) and leaf area index (LAI) estimates used in this study as predictors of final grain yield, separately for each crop. These include canopy chlorophyll metrics, which were shown to be more sensitive to high green LAI values than NDVI (Viña et al., 2011), alongside STI and NDTI, which are related to dry biomass (Jacques et al., 2014; Renier et al., 2015).

The LAI comes from the Sen2-Agri system (Bontemps et al., 2015) where it is estimated using an artificial neural network inversion of the PROSAIL radiative transfer model based on Sentinel-2 data (Bontemps et al., 2015). Theoretically, using a full VI seasonal integral (rather than a subset thereof) should deliver higher prediction skill for crop yield, as the end result of a highly non-linear plant development and growth process. In practice, the downgraded overpass frequency imposed by Sentinel2's incomplete deployment in 2016 limited the number of available tiles to 6. In the absence of detailed management information for each individual field used for yield model calibration, and given the large intra-specific variability in crop phenologies, we limited ourselves to peak VI (and LAI) as the sole predictor against which yield measurements are regressed. The potential of this approach has already been demonstrated elsewhere (Azzari et al., 2017; Becker-Reshef et al., 2010; Jain et al., 2016).

For each species, yield regression models were calibrated using the most homogeneous half of the fields monitored, defined as fields located on dominant soils (sandy, loamy, and clayey) and within which heterogeneity in measured yield is lower than the 66*th* percentile. As for crop type classification, a 10-m internal buffer and a tree mask were applied - before VI and LAI extraction - to all studied fields in order to rely on a '*pure*' predictor. Due to fieldwork constraints (peanut harvest completed at the time of field campaign), only the four dominant crop types (cotton, maize, millet and sorghum) are involved in yield estimation. The determination coefficient (R^2) computed for each linear regression serves as performance indicator. The yield regression models are validated using the complete data set by computing RMSE, variance and standard deviation (S_j).

4.3. Production estimation

Uncertainties inherent to the crop type classification and to the yield estimation are combined for unbiased production estimates using a Monte Carlo approach with 100 realizations, as follows. For each pixel classified as crop type *i*, each realization draws a random crop type *j* constrained by $P(j|i)$ as derived from the confusion matrix, then applies the corresponding stochastic yield model with a Gaussian, zero-mean error term ϵ_j (Eq. (2)).

$$\widehat{y_j} = \alpha_j * LAI_{peak} + \beta_j + \epsilon_j \quad with\ \epsilon_j \approx \mathcal{N}(0, S_j) \tag{2}$$

With α_j, β_j the coefficients of the yield linear regressions for each crop type *j*; ϵ_j the error on those regressions and $\widehat{y_j}$ one potential realization of yield for a pixel of crop type *j*. The estimated yields are truncated at 0 and 10 t/ha which represents extreme theoretical values for yield in these regions. The production estimate then corresponds to the averaging across all 100 realizations of crop yields multiplied by corresponding crop area. The standard deviation of the 100 simulations of production estimates is computed and expressed the model uncertainty for crop production estimates.

5. Results and discussion

5.1. Crop type classification

5.1.1. Accuracy of the crop type map and the resulting crop type area

The OA of the pixel-based crop type map reaches 80.16 (± 0.27)%. After parcel filtering, it increases to 85.5 (± 0.23)% (Table 2). The cotton crop, covering more than 40% of the cropland, is the most reliably mapped (Fscore: 93.86%), followed by maize (Fscore: 87.52%) and millet (Fscore: 82.5%). The cotton vegetative cover differs significantly from other crops making the discrimination easier. Sorghum is the least well classified with Fscore of only 45.7%. Strong misclassifications occur between sorghum and millet, which was expected due to the reasonably large calendar overlap. Pooling millet and sorghum into a single target class increases the OA to 91%. High weed infestation levels in peanut are often associated with prominent intra-field heterogeneity, leading to high omission error (PA = 55.07%). Conversely, no commission error is observed because well weeded peanut fields have a distinct spectral and temporal signature (Table 2). The confusion between millet and cotton is also noteworthy (444 misclassified cotton pixels).

Table 2
Confusion matrix for the crop type map after object filtering. Map categories are the rows while the reference categories are the columns (n = 22,591).

	Cotton	Maize	Millet	Sorghum	Peanut	Other	UA [%]
Cotton	9416	356	126	196	56	18	92.6
Maize	3	3986	88	255	64	138	87.91
Millet	444	196	5005	1095	13	23	73.86
Sorghum	32	37	141	740	0	0	77.89
Peanut	0	0	0	0	163	0	100
Other	0	0	0	0	0	0	/
PA [%]	95.16	87.13	93.38	32.37	55.07	0	OA = 85.48

Generally, our findings are congruent with the expression of differential phenotypic traits (plant phenology, canopy architecture) and management practices (sowing date, density, weeding) between dominant crops. Maize, a common stop-gap crop, is typically senescent well ahead of other species making classification easier. The thickness of cotton and millet canopies tend to homogenize crop response at the field scale, in contrast to other species. Peanut features the broadest range of weed infestation and thus reveals stark differences in household labor constraints later in the season. Sorghum, a typical frontier crop planted on more marginal soils with the least fertilizer input of all, expresses the highest within-field heterogeneity among the dominant crops.

Fig. 3 presents the resulting crop type map.

From top to bottom, the false color Sentinel-2, the crop type classification and the crop type classification after object filtering are shown in zooms for two different sites of the study area.

In spite of the complex modulation of systematic environmental gradients by local management halos centered on separate smallholder farm households, the crop map produced corroborates the explicit environmental determinism guiding spatial crop allocation in rainfed systems (Fig. 4). On each farm, cash crop (cotton) and highly-fertilized crops (cotton, maize) are preferably cultivated on more finely textured soils with the highest water holding capacity (WHC), and highest fertility. Millet, which is a more valuable and valued commodity than sorghum for both self-consumption and (in the foreseeable future) sales, is typically also inserted on the same parcels in rotation, benefiting from fertility carry-over effects. Sorghum, a robust and phenologically plastic crop is more frequently targeted to more marginal environments (such as rocky soil), although it is also often substituted for millet in rotations after cotton and maize.

The unbiased crop type area is computed for each village within the Koningue commune (Fig. 5). Maize and cotton crops reflect only small area differences between the pixel counting area estimate and the unbiased area estimate, as their classification accuracy is high, in contrast with the often-confused millet and sorghum crops. Reflecting population and cultivated area sizes, Sukumba features the largest crop area for any species (total cultivated area: 8899 ha), and Ngueguesso1 the smallest (entire cultivated area: 523 ha). While at comparable total cultivated areas, Banesso (3146 ha) and Dougan (2925 ha) respectively

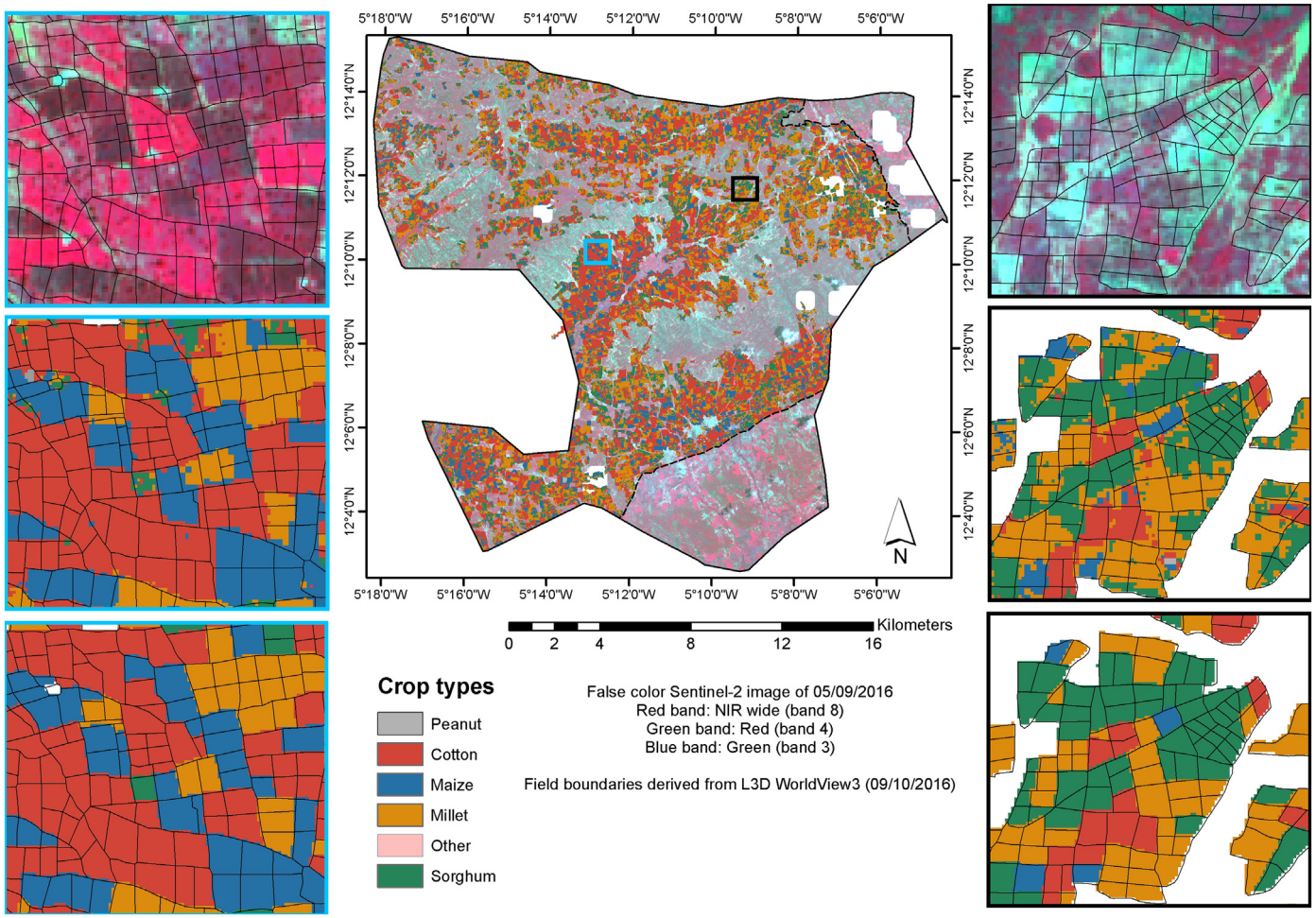

Fig. 3. Crop type map over the study area produced with Random Forest classification based on Sentinel-2 time series. Zooms-ins are done on two different areas of the image and show, from top to bottom, the false color Sentinel-2 (9 September 2016), and the crop type classification before and after object filtering.

feature more cotton and maize, and more millet and sorghum reflecting the higher proportion of high (low) WHC soils in Banesso lowlands (Dougan highlands).

5.1.2. *Bands and dates importance for crop type discrimination*

According to the Gini Index and as illustrated in Fig. 6, red-edge and near infrared (NIR) reflectances for late-season acquisitions (Sept. 5, Oct. 5) contribute most to the crop type classification accuracy in the study area. Unfortunately, the first available low cloud-coverage image was acquired at the end of July 2016, excluding the start of season from the analysis.

The usefulness of red-edge and NIR bands corroborates earlier conclusions by Immitzer et al. (2016). The importance of the end-of-season dates might explain part of the confusion between millet and cotton because this period emphasizes similarities between the two species (canopy thickness, spherical to planophile leaf angle distribution functions) at the expense of differences. Given the limited number of cloud-free acquisitions during the 2016 cropping season, and the inter-annual variability in weather and farmers responsive management, drawing a definitive conclusion on the best week for crop type mapping is probably too ambitious. However, targeting the peak LAI period in September is a pragmatic option in this production system.

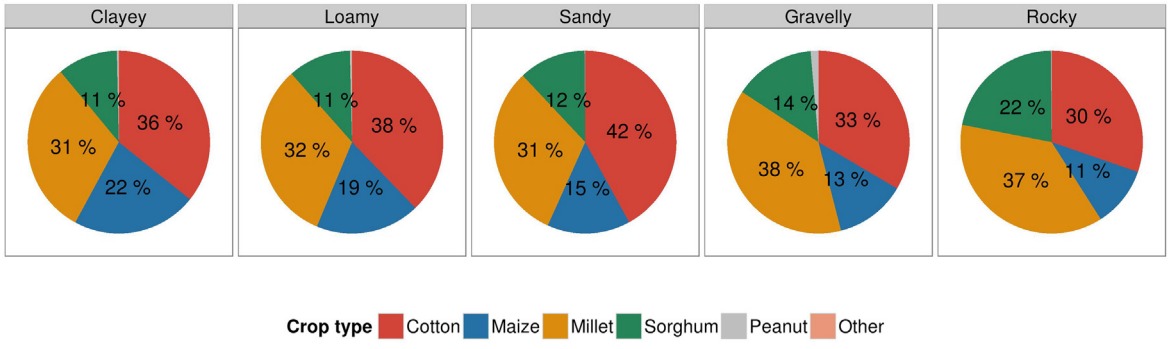

Fig. 4. Distribution of the crops according to the vernacular soil map.

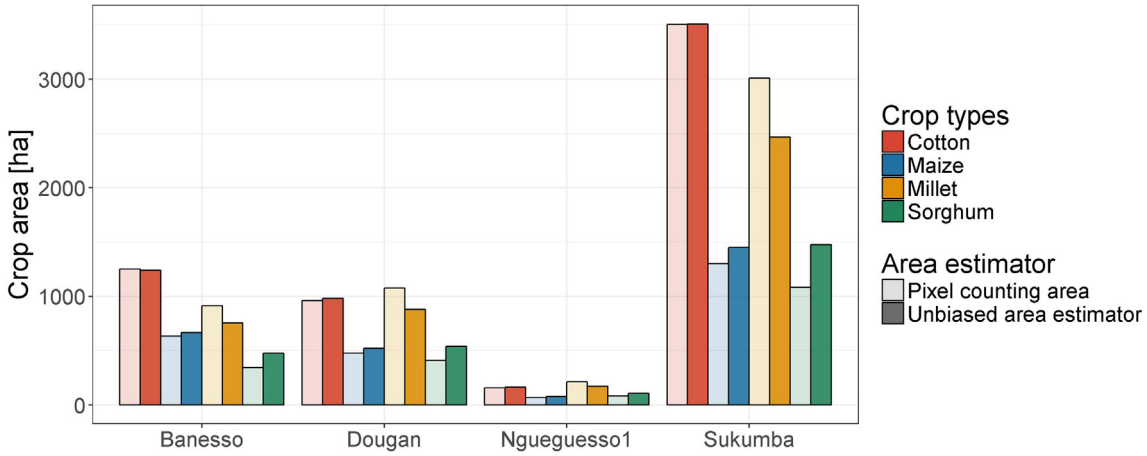

Fig. 5. Crop area estimate for each village with the pixel counting approach and the unbiased area estimator.

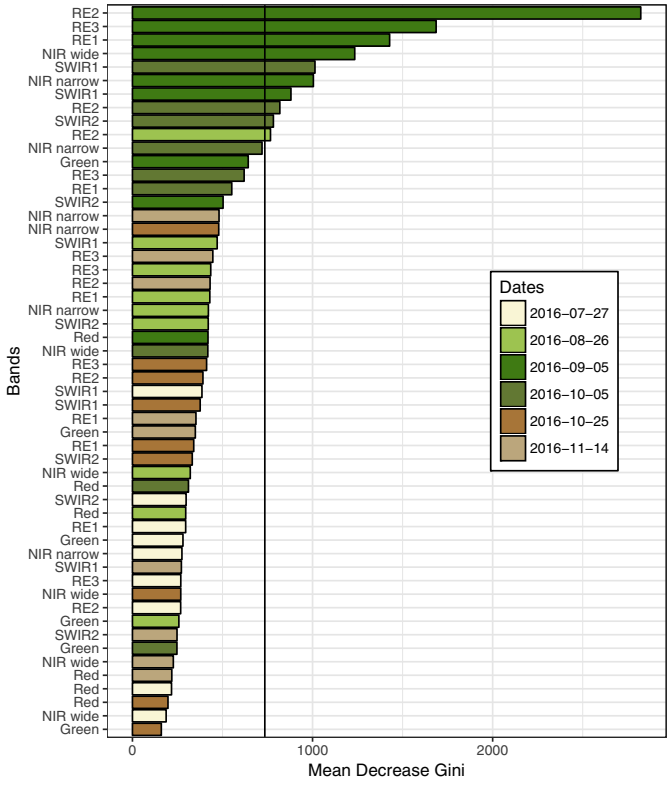

Fig. 6. Features (band x date) importance for crop type classification. The vertical line corresponds to the mean decrease in Gini Index across features considered. The following acronyms are used for the Sentinel-2 bands: three bands in the red edge (RE1, RE2, RE3), two bands in the NIR (NIR wide and NIR narrow) and two bands in the short wave infrared (SWIR1, SWIR2). For more information on the bands description, please refer to Clevers and Gitelson (2013).

5.1.3. Impact of in-field trees on crop type classification

The Sentinel-2 tree mask resampled from VHR tree mask (Fig. 7) shows high performance with OA of 94.67% and Fscore for tree and non-tree of 95.58% and 92.3%, respectively.

Removal of the trees footprint from the classification inputs leads to a small decay in OA (from 80.16% to 79.99%), which remains within the map's standard deviation (± 0.27%). We consequently suggest that trees removal is not required for crop type mapping at 10-m spatial resolution in the study area. This finding is consistent with the fact that the preeminence of end-of-season dates in the classification approach reduces the spectral differences between tree and crop pixels as crops are at their maximum of vegetation growth. Besides, while it systematically varies along the catena and as a function of distance to main settlements, residual tree density remains independent of the crop type in a production system very dominantly based on inter-annual crop rotations.

5.2. Yield estimation

Fig. 8 reports the strength of crop-specific linear regressions between field measurements of grain yield and total AGB. Very high R^2's are observed for maize and millet (0.85 and 0.84 respectively).

Cotton being an indeterminate crop displayed a weaker AGB-yield relationship ($R^2 = 0.68$), as only one destructive sampling of cotton bolls was possible which may have under-sampled the amount of reproductive material generated. Contributing factors to low R^2 for sorghum (0.62) could include the typically wider range of soil types (notably marginal soils) and low fertilization rates. The best yield estimator differs for each crop type (Fig. 9). Nevertheless, on the average across crop types, LAI outperforms VIs for yield estimation (average $R^2 = 0.64$ in comparison with peak NDVI reaching an average R^2 of 0.44). The superior performance of LAI can be explained in part by its higher sensitivity in conditions of higher vegetation biomass (when most VIs saturate).

For yield estimation, the highest R^2 is reached for millet followed by cotton and maize. Sorghum shows lower R^2 which can be linked to lower AGB - yield relationship ($R^2 = 0.616$) (Fig. 8). In fact, as sorghum is often cultivated on shallow soils, low water availability can affect both plant maintenance and grain filling in various proportions. Further, sorghum is often strongly photoperiod sensitive, with amounts of AGB generated function of its very variable sowing date, which typically spans up to 6 weeks in a single landscape. A highly photoperiodic sorghum planted early would not only feature a depressed harvest index due to its lengthened vegetative phase, it could also further depress grain yield due to competing allocation of residual soil water for biomass maintenance during the grain filling stage. Finally, significant agro-biodiversity is actively maintained by farmers, expressing mostly in sorghum with easily 3–4 contrasting genotypes being employed by farmers in response to various stressors and tactical opportunities. All these factors contribute to decouple sorghum grain yield from AGB, affecting in turn the correlation of yield and satellite-derived LAI.

Crop specific yield linear regressions were calibrated on a homogeneous subset of the field data to limit the impact of the ground measurements heterogeneity and errors. Linear regressions between peak LAI and in situ yield averaged at parcel level for each crop type are shown in Fig. 10.

Depending on the crop, these explained between 48 to 80% of yield

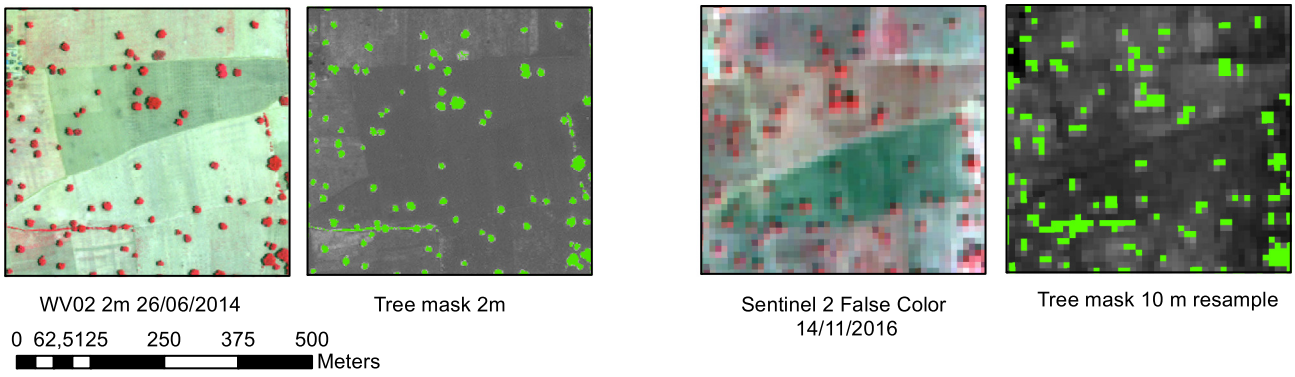

Fig. 7. Tree mask based on VHR image at the beginning of 2014 growing season (26/06/2014) and resampled to 10-m to match Sentinel-2 resolution. Both satellite images are presented in false colors.

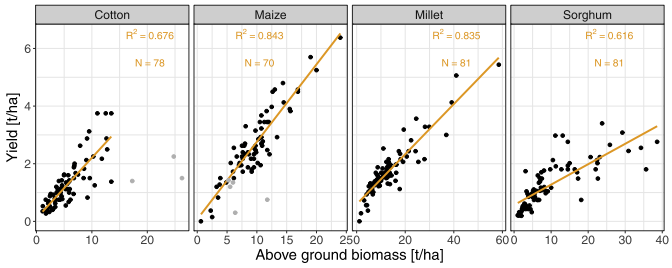

Fig. 8. Linear regression between yield and total above ground biomass as measured in situ on 4 m^2 plots for each crop type. The outliers are colored in gray and removed from regressions.

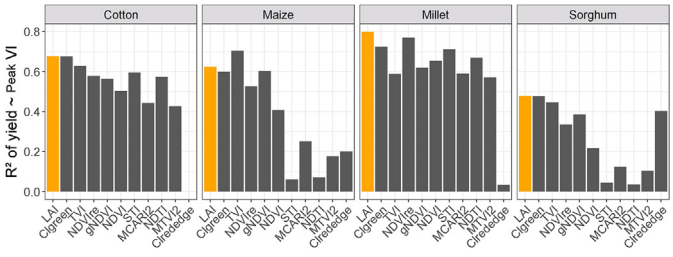

Fig. 9. R^2 of the linear regressions between yield and peak VI's.

Table 3
Linear regression for yield estimation and its validation.

	Equation	RMSE	σ^2
Cotton	*Yield [t/ha]* = −0.03 + 0.77 * *peak LAI*	0.5	0.25
Maize	*Yield [t/ha]* = −1.04 + 1.93 * *peak LAI*	0.97	0.99
Millet	*Yield [t/ha]* = 0.39 + 1.03 * *peak LAI*	0.62	0.39
Sorghum	*Yield [t/ha]* = −1.56 + 2.66 * *peak LAI*	0.73	0.47

variability over the calibration fields. RMSE varied from 0.5 to 1 t/ha for the different crops, in a context of wide yield ranges from 1 to 6 t/ha (Table 3). As the peak LAI is reached around the end of August and harvest starts – for most studied crops – at the end of September, the peak LAI provides yield estimation at least one month ahead harvest.

5.3. Agricultural production estimate

The Monte Carlo combination of crop type and yield estimates provides aggregate figures of crop-specific production by village (Fig. 11). Given the considerable differences in cultivated area, the crop production levels differ strongly across villages. The highest inter-village variation in yield is observed for maize. Ngueguesso 1 displays the highest maize and cotton yields. Potential explanations may include the

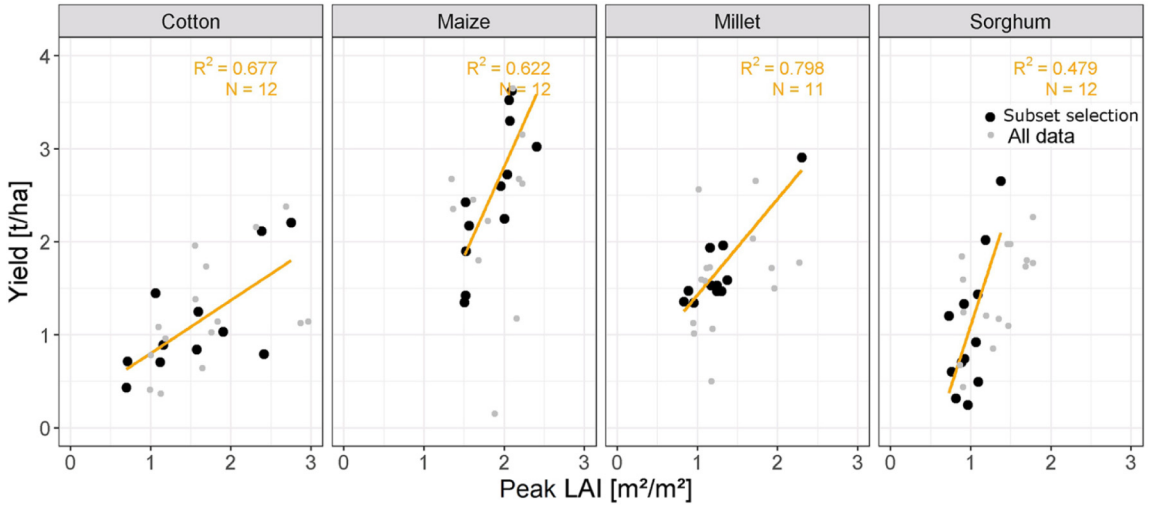

Fig. 10. Linear regressions between peak LAI and yield for each crop type. These regressions are calibrated on a subset (black dots) composed of the more homogeneous fields.

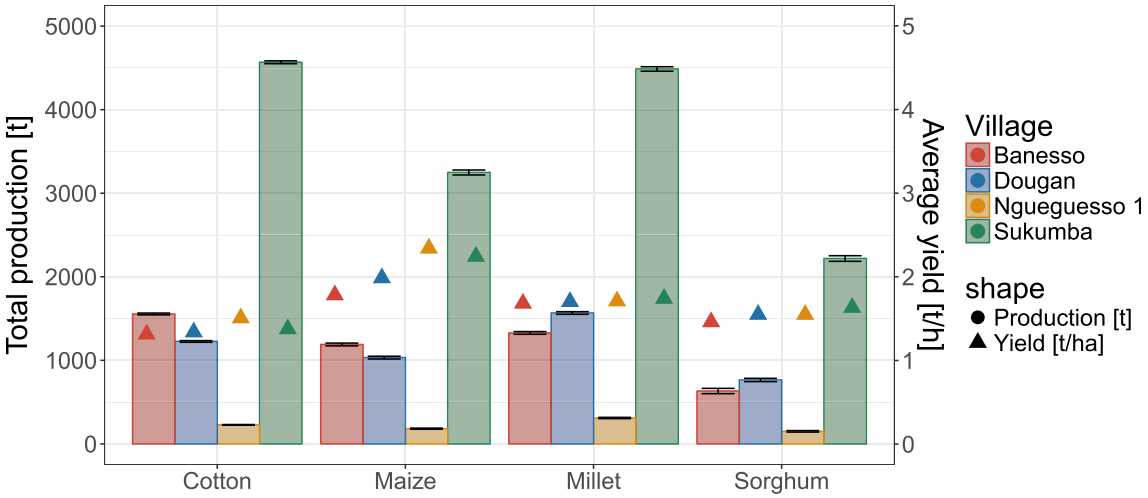

Fig. 11. Total production (bar plot) and average yield (point plot) for each crop type and each village. Error bars represent 5 times the standard deviation on production estimate with the Monte Carlo approach.

Table 4
Standard deviation and uncertainty (%) of crop production estimate model by the Monte Carlo approach for each crop type and village, in tons.

Standard deviation [t] Uncertainty [%]	Banesso	Dougan	Ngueguesso1	Sukumba
Cotton	2.19 (0.03%)	1.97 (0.04%)	0.76 (0.08%)	3.42 (0.019%)
Maize	3.32 (0.07%)	3.31 (0.08%)	1.35 (0.18%)	5.94 (0.05%)
Millet	3.24 (0.06%)	3.14 (0.05%)	1.54 (0.12%)	5.32 (0.03%)
Sorghum	3.66 (0.14%)	3.92 (0.13%)	1.79 (0.3%)	6.72 (0.08%)

widely documented trend towards ‘ *maizification*’ of cereal cultivation in Mali's cotton belt, combined with higher response of maize to fertilization, higher vulnerability to low soil fertility, and substantial fertility carry-over in the locally dominant cotton-maize-(another crop) tri-annual rotation scheme.

Aggregation of production values estimated through the Monte Carlo approach results in low uncertainty of model estimate for all crop types and villages (Table 4). Higher uncertainties are met in Ngueguesso1 due to smaller cultivated area, which increases error when aggregating at village level. Due to their lower Fscore in the classification, sorghum features higher production uncertainties. The actual error of the production estimate could only be assessed by comparison with accurate official agricultural statistics available only at a higher level of aggregation (*i.e.* Mali's circle).

6. Conclusion

This paper proposes an integrated approach to estimate, using Sentinel-2 data, crop-specific production at a community level based on the combination of crop type classification, unbiased area estimate and remotely sensed yield predictors in a stochastic framework. Production estimates generated demonstrate a robust skill, featuring no more than 0.3% of model uncertainty on total production for one community and one crop type.

The recent Sentinel-2 mission opens up new prospects for food security and agricultural performance monitoring in smallholder farming systems. Subject to the availability of a field dataset (crop type polygons to train the classification), high-resolution imagery (as Sentinel-2) appears sufficient to accurately classify crop type in the relatively ‘ simple’ smallholder farming systems of Mali's cotton belt (OA = 80%). The use of 2-m VHR images for object filtering improved OA by 5%. Those results were obtained inside a cropland mask derived from VHR imagery. Nevertheless, we believe that accurate cropland mask could be obtained directly from Sentinel-2 data such as demonstrated using the Sen-2-Agri system.

Remote sensing estimates of peak LAI outperformed all spectral VIs tested for yield estimation. The particular value of a single peak LAI predictor is that it offers yield estimation one month ahead of harvest. While the doubling of acquisition frequency brought about by the launch of Sentinel-2B in 2017 may result in an LAI time integral outperforming peak LAI for yield estimation, possible accuracy and/or lead time improvements will need to be evaluated against increased computing costs. While the growing period obviously involves high and persistent cloud coverage, preliminary evidence indicates that Sentinel-2B effectively increases the likelihood of a successful < 20% cloud cover image acquisition in the Sudano-Sahelian region. Although this evidence remains anecdotal so far, a peak biomass approach such as the one proposed here may offer a sufficiently robust, agile and scalable option for early and granular estimates of crop production.

While estimates of aggregate production are expected to improve our ability to monitor community-level food security accurately, the clear resolution of intra-landscape variability in production levels may even, more importantly, lead to better targeting of agricultural development interventions, addressing the actual bottlenecks of smallholder productivity improvement such as fertilization gaps (Schut et al., 2018). Indeed, agricultural development interventions such as fertilizer or seed supply, microcredit, market access, livestock support, diversification and off-farm activities often follow one-size-fits-all approaches which are unlikely to address the diverse socio-economic and biophysical production conditions in heterogeneous smallholder systems. Efficient, granular baseline mapping of smallholder production levels offers the perspective of a truly transformative environment for the agricultural intensification required to meet food security and enhanced livelihood targets.

Acknowledgments

This research was funded by a FNRS (Fonds National de Recherche Scientifique belge) grant for M-J Lambert. The field campaign realized by M-J Lambert in October and November 2016 was financed by the FNRS short stay abroad. The success of the field campaign largely depended upon the collaborations with ICRISAT (in particular Pierre Sibiry Traoré, Issa Kassogue and Kadiatou Touré) and the AMEDD NGO (Birama Sissoko, Gilbert Dembélé, and all the field operators). This

publication was made possible (in part) by the STARS project, an integrated effort to improve our understanding of the use of remote sensing technology in monitoring smallholder farming supported by the Bill and Melinda Gates Foundation. Additional support was provided by the CGIAR Research Program on Climate Change, Agriculture and Food Security (CCAFS) (please refers to https://ccafs.cgiar.org/donors for information about the fundings). The authors also acknowledge the critical provision of digitized field vector layers by the Université de Sherbrooke.

References

Akponikpe, P., Minet, J., Gerard, B., Defourny, P., Bielders, C., 2011. Spatial fields dispersion as a farmer strategy to reduce agro-climatic risk at the household level in pearl millet-based systems in the Sahel: a modeling perspective. Agric. For. Meteorol. 151 (2), 215–227.

Azzari, G., Jain, M., Lobell, D.B., 2017. Towards fine resolution global maps of crop yields: testing multiple methods and satellites in three countries. Remote Sens. Environ. 202, 129–141.

Baffes, J., 2007. Distortions to cotton sector incentives. In: Distortions to cotton incentives in Benin, Burkina Faso, Chad, Mali, and Togo.

Baruth, B., Royer, A., Klisch, A., Genovese, G., 2008. The use of remote sensing within the mars crop yield monitoring system of the European Commission. Int. Arch. Photogramm. Remote Sens. Spat. Inf. Sci. 37, 935–940.

Becker-Reshef, I., Vermote, E., Lindeman, M., Justice, C., 2010. A generalized regression-based model for forecasting winter wheat yields in Kansas and Ukraine using modis data. Remote Sens. Environ. 114 (6), 1312–1323.

Blaes, X., Chomé, G., Lambert, M.-J., Traoré, P.S., Schut, A.G., Defourny, P., 2016. Quantifying fertilizer application response variability with VHR satellite NDVI time series in a rainfed smallholder cropping system of Mali. Remote Sens. 8 (6), 531.

Bontemps, S., Arias, M., Cara, C., Dedieu, G., Guzzonato, E., Hagolle, O., Inglada, J., Matton, N., Morin, D., Popescu, R., Rabaute, T., Savinaud, M., Sepulcre, G., Valero, S., Ahmad, I., Bégué, A., Wu, B., de Abelleyra, D., Diarra, A., Dupuy, S., French, A., ul Hassan Akhtar, I., Kussul, N., Lebourgeois, V., Le Page, M., Newby, T., Savin, I., Verón, S.R., Koetz, B., Defourny, P., 2015. Building a data set over 12 globally distributed sites to support the development of agriculture monitoring applications with sentinel-2. Remote Sens. 7 (12), 16062–16090.

Breiman, L., 2001. Random forests. Mach. Learn. 45 (1), 5–32.

Breusers, M., 2004. Responses to climate variability in the Kaya region, Burkina Faso. In: The Impact of Climate Change on Drylands. Springer, pp. 207–241.

Broge, N.H., Leblanc, E., 2001. Comparing prediction power and stability of broadband and hyperspectral vegetation indices for estimation of green leaf area index and canopy chlorophyll density. Remote Sens. Environ. 76 (2), 156–172.

Burke, M., Lobell, D.B., 2017. Satellite-based assessment of yield variation and its determinants in smallholder african systems. Proc. Natl. Acad. Sci. 114 (9), 2189–2194.

Chivasa, W., Mutanga, O., Biradar, C., 2017. Application of remote sensing in estimating maize grain yield in heterogeneous African agricultural landscapes: a review. Int. J. Remote Sens. 38 (23), 6816–6845.

Clevers, J.G., Gitelson, A.A., 2013. Remote estimation of crop and grass chlorophyll and nitrogen content using red-edge bands on sentinel-2 and-3. Int. J. Appl. Earth Obs. Geoinf. 23, 344–351.

Cousins, B., 2010. What is a 'Smallholder'? In: Working Paper. 16 PLAAS, University of the Western Cape.

Debats, S.R., Luo, D., Estes, L.D., Fuchs, T.J., Caylor, K.K., 2016. A generalized computer vision approach to mapping crop fields in heterogeneous agricultural landscapes. Remote Sens. Environ. 179, 210–221.

Delrue, J., Bydekerke, L., Eerens, H., Gilliams, S., Piccard, I., Swinnen, E., 2013. Crop mapping in countries with small-scale farming: a case study for West Shewa, Ethiopia. Int. J. Remote Sens. 34 (7), 2566–2582.

Devereux, S., 2009. Why does famine persist in Africa? Food Sec. 1 (1), 25.

Diallo, D., Keita, D., 1995. Un système paysan de classement des sols dans la zone agroécologique du djitoumou, mali. Cahiers Agricultures 4 (5), 371–375.

Dixon, J., Taniguchi, K., Wattenbach, H., TanyeriArbur, A., 2004. Smallholders, Globalization and Policy Analysis. vol. 5 Food Agriculture Org.

Falconnier, G., 2009. Quelles évolutions possibles pour les exploitations agricoles familiales du Sud du Mali face à la crise de la filière cotonnière. Ph.D. thesis. Master Thesis, ESAT 1 DAT Montpellier Supagro-Irc 70p.

Gaiser, T., Judex, M., Hiepe, C., Kuhn, A., 2010. Regional simulation of maize production in tropical savanna fallow systems as affected by fallow availability. Agric. Syst. 103 (9), 656–665.

Gallego, F.J., 2004. Remote sensing and land cover area estimation. Int. J. Remote Sens. 25 (15), 3019–3047.

Genesio, L., Bacci, M., Baron, C., Diarra, B., Di Vecchia, A., Alhassane, A., Hassane, I., Ndiaye, M., Philippon, N., Tarchiani, V., et al., 2011. Early warning systems for food security in West Africa: evolution, achievements and challenges. Atmos. Sci. Lett. 12 (1), 142–148.

Gislason, P.O., Benediktsson, J.A., Sveinsson, J.R., 2006. Random forests for land cover classification. Pattern Recogn. Lett. 27 (4), 294–300.

Gitelson, A., Merzlyak, M.N., 1994. Spectral reflectance changes associated with autumn senescence of *Aesculus hippocastanum* L. and *Acer platanoides* L. leaves. spectral features and relation to chlorophyll estimation. J. Plant Physiol. 143 (3), 286–292.

Gitelson, A.A., Kaufman, Y.J., Merzlyak, M.N., 1996. Use of a green channel in remote sensing of global vegetation from EOS-MODIS. Remote Sens. Environ. 58 (3), 289–298.

Gitelson, A.A., Viña, A., Arkebauer, T.J., Rundquist, D.C., Keydan, G., Leavitt, B., 2003. Remote estimation of leaf area index and green leaf biomass in maize canopies. Geophys. Res. Lett. 30 (5), 1248–1251.

Haboudane, D., Miller, J.R., Pattey, E., Zarco-Tejada, P.J., Strachan, I.B., 2004. Hyperspectral vegetation indices and novel algorithms for predicting green LAI of crop canopies: modeling and validation in the context of precision agriculture. Remote Sens. Environ. 90 (3), 337–352.

Hagolle, O., Huc, M., Pascual, D.V., Dedieu, G., 2010. A multi-temporal method for cloud detection, applied to formosat-2, venμs, landsat and sentinel-2 images. Remote Sens. Environ. 114 (8), 1747–1755.

Hagolle, O., Huc, M., Villa Pascual, D., Dedieu, G., 2015. A multi-temporal and multi-spectral method to estimate aerosol optical thickness over land, for the atmospheric correction of formosat-2, landsat, venμs and sentinel-2 images. Remote Sens. 7 (3), 2668–2691.

Han, J., Wei, C., Chen, Y., Liu, W., Song, P., Zhang, D., Wang, A., Song, X., Wang, X., Huang, J., 2017. Mapping above-ground biomass of winter oilseed rape using high spatial resolution satellite data at parcel scale under waterlogging conditions. Remote Sens. 9 (3), 238.

Hastie, T., Tibshirani, R., Friedman, J., 2009. Unsupervised learning. In: The Elements of Statistical Learning. Springer, pp. 485–585.

Immitzer, M., Vuolo, F., Atzberger, C., 2016. First experience with sentinel-2 data for crop and tree species classifications in Central Europe. Remote Sens. 8 (3), 166.

Jacques, D.C., Kergoat, L., Hiernaux, P., Mougin, E., Defourny, P., 2014. Monitoring dry vegetation masses in semi-arid areas with modis SWIR bands. Remote Sens. Environ. 153, 40–49.

Jain, M., Srivastava, A.K., Joon, R.K., McDonald, A., Royal, K., Lisaius, M.C., Lobell, D.B., et al., 2016. Mapping smallholder wheat yields and sowing dates using micro-satellite data. Remote Sens. 8 (10), 860.

Jia, K., Liang, S., Wei, X., Yao, Y., Su, Y., Jiang, B., Wang, X., 2014. Land cover classification of landsat data with phenological features extracted from time series modis NDVI data. Remote Sens. 6 (11), 11518–11532.

Jin, Z., Azzari, G., Burke, M., Aston, S., Lobell, D.B., 2017. Mapping smallholder yield heterogeneity at multiple scales in Eastern Africa. Remote Sens. 9 (9).

Karlson, M., Ostwald, M., 2015. Remote sensing of vegetation in the Sudano-Sahelian zone: a literature review from 1975 to 2014. J. Arid Environ. 124, 257–269.

Laris, P., Foltz, J.D., Voorhees, B., 2015. Taking from cotton to grow maize: the shifting practices of small-holder farmers in the cotton belt of Mali. Agric. Syst. 133, 1–13.

Lebourgeois, V., Dupuy, S., Vintrou, É., Ameline, M., Butler, S., Bégué, A., 2017. A combined random forest and obia classification scheme for mapping smallholder agriculture at different nomenclature levels using multisource data (simulated sentinel-2 time series, VHRS and DEM). Remote Sens. 9 (3), 259.

Leroux, L., Jolivot, A., Bégué, A., Seen, D.L., Zoungrana, B., 2014. How reliable is the modis land cover product for crop mapping sub-Saharan agricultural landscapes? Remote Sens. 6 (9), 8541–8564.

Maxwell, D., 2002. Why do famines persist? IDS Bull. 33 (4), 48–54.

McCarty, J., Neigh, C., Carroll, M., Wooten, M., 2017. Extracting smallholder cropped area in Tigray, Ethiopia with wall-to-wall sub-meter worldview and moderate resolution landsat 8 imagery. Remote Sens. Environ.

Morel, J., Todoroff, P., Bégué, A., Bury, A., Martiné, J.-F., Petit, M., 2014. Toward a satellite-based system of sugarcane yield estimation and forecasting in smallholder farming conditions: a case study on Reunion Island. Remote Sens. 6 (7), 6620–6635.

Morton, J.F., 2007. The impact of climate change on smallholder and subsistence agriculture. Proc. Natl. Acad. Sci. 104 (50), 19680–19685.

Pervez, M.S., Budde, M., Rowland, J., 2014. Mapping irrigated areas in Afghanistan over the past decade using modis NDVI. Remote Sens. Environ. 149, 155–165.

Potts, M., Zulu, E., Wehner, M., Castillo, F., Henderson, C., 2013. Crisis in the Sahel: possible solutions and the consequences of inaction. The OASIS Initiative.

Renier, C., Waldner, F., Jacques, D.C., Babah Ebbe, M.A., Cressman, K., Defourny, P., 2015. A dynamic vegetation senescence indicator for near-real-time desert locust habitat monitoring with modis. Remote Sens. 7 (6), 7545–7570.

Rodriguez-Galiano, V.F., Ghimire, B., Rogan, J., Chica-Olmo, M., Rigol-Sanchez, J.P., 2012. An assessment of the effectiveness of a random forest classifier for land-cover classification. ISPRS J. Photogramm. Remote Sens. 67, 93–104.

Rossiter, D., 2004. Technical note: statistical methods for accuracy assessment of classified thematic maps. Enschede (NL): International Institute for Geo-information Science & Earth Observation (ITC) 25 (92), 107.

Rouse Jr., J., Haas, R., Schell, J., Deering, D., 1974. Monitoring vegetation systems in the Great Plains with ERTS. NASA special publication 351, 309.

Schut, A.G., Traore, P.C.S., Blaes, X., de By, R.A., 2018. Assessing yield and fertilizer response in heterogeneous smallholder fields with UAVs and satellites. Field Crop Res. 221, 98–107.

Srivastava, A.K., Mboh, C.M., Gaiser, T., Webber, H., Ewert, F., 2016. Effect of sowing date distributions on simulation of maize yields at regional scale a case study in central Ghana, West Africa. Agric. Syst. 147, 10–23.

Sweeney, S., Ruseva, T., Estes, L., Evans, T., 2015. Mapping cropland in smallholder-dominated savannas: integrating remote sensing techniques and probabilistic modeling. Remote Sens. 7 (11), 15295–15317.

Traoré, K., 2003. Le parc à karité: sa contribution à la durabilité de la-grosystème. Cas dune toposéquence à Konobougou (Mali-Sud). Ph.D. thesis. Thèse, école nationale supérieure agronomique de Montpellier (Ensam).

Traoré, K., McCarthy, G., Gigou, J., Doumbia, M., Bagayoko, A., Yost, R., Konaré, H., Dioni, L., Coulibaly, H., Sidibé, A., et al., 2002. Aménagement en courbes de niveau et conservation du carbone. In: Colloque International, Gestion de la biomasse, ruissellement, érosion et séquestration du carbone, pp. 24–28.

Traroé, P.C.S, Annerose, D., Goita, K., 2015. STARS-ISABELA 2014-2015, Parcel database validation protocol, V1. STARS.
Van Deventer, A., Ward, A., Gowda, P., Lyon, J., 1997. Using thematic mapper data to identify contrasting soil plains and tillage practices. Photogramm. Eng. Remote. Sens. 63, 87–93.
Vancutsem, C., Marinho, E., Kayitakire, F., See, L., Fritz, S., 2012. Harmonizing and combining existing land cover/land use datasets for cropland area monitoring at the African continental scale. Remote Sens. 5 (1), 19–41.
Viña, A., Gitelson, A.A., Nguy-Robertson, A.L., Peng, Y., 2011. Comparison of different vegetation indices for the remote assessment of green leaf area index of crops. Remote Sens. Environ. 115 (12), 3468–3478.
Weiss, M., Baret, F., 1999. Evaluation of canopy biophysical variable retrieval performances from the accumulation of large swath satellite data. Remote Sens. Environ. 70 (3), 293–306.